

ARTICLE

Ventral subiculum promotes wakefulness through several pathways in male mice

Xue-Fen Zhang^{1,5}, Yi-Dan Li^{1,5}, Yue Li¹, Ying Li¹, Dan Xu², Lin-Lin Bi^{3,4}✉ and Hai-Bo Xu¹✉

© The Author(s), under exclusive licence to American College of Neuropsychopharmacology 2024

The ventral subiculum (vSUB), the major output structure of the hippocampal formation, regulates motivation, stress integration, and anxiety-like behaviors that rely on heightened arousal. However, the roles and underlying neural circuits of the vSUB in wakefulness are poorly known. Using *in vivo* fiber photometry and multichannel electrophysiological recordings in mice, we found that the vSUB glutamatergic neurons exhibited high activities during wakefulness. Moreover, activation of vSUB glutamatergic neurons caused an increase in wakefulness and anxiety-like behaviors and induced a rapid transition from sleep to wakefulness. In addition, optogenetic stimulation of vSUB glutamatergic terminals and retrograde-targeted chemogenetic activation of vSUB glutamatergic neurons revealed that vSUB promoted arousal by innervating the lateral hypothalamus (LH), nucleus accumbens (NAc) shell, and prefrontal cortex (PFC). Nevertheless, local microinjection of dopamine D1 or D2/D3 receptor antagonist blocked the wake-promoting effect induced by chemogenetic activation of vSUB pathways. Finally, chemogenetic inhibition of vSUB glutamatergic neurons decreased arousal. Altogether, our findings reveal a prominent contribution of vSUB glutamatergic neurons to the control of wakefulness through several pathways.

Neuropsychopharmacology (2024) 49:1468–1480; <https://doi.org/10.1038/s41386-024-01875-6>

INTRODUCTION

The ventral subiculum (vSUB) is the main ventral hippocampal (vHPC) output region and plays a critical role in stress integration [1], anxiety-like behaviors [2, 3], and spatial learning and memory [4, 5]. Arousal and wakefulness are fundamental properties of such adaptive behaviors. Dysfunction of the vSUB is associated with schizophrenia [6, 7] and drug seeking [8–10], which are often accompanied by symptoms of sleep disturbances [11]. Early electrophysiological findings suggest that sleep states can differentiate single-unit activity recorded from human SUB [12]. Moreover, lesions of the entorhinal cortex and SUB increase daytime slow wave sleep (SWS) but decrease rapid eye movement (REM) sleep [13]. People with obstructive sleep apnea show an increase in regional volume in CA1 and SUB relative to controls [14]. In addition, both suboptimal sleep and stress may synergistically contribute to hippocampal subfield damage and structural changes (including the SUB) [15]. These findings led to the hypothesis that the vSUB may be involved in sleep–wake regulation. However, whether the vSUB participates in the regulation of the sleep–wake cycle is poorly investigated.

The vSUB is composed of heterogenous neuronal populations with parallel, long-range axonal projections to various cortical and subcortical regions implicated in sleep–wake regulation, including the nucleus accumbens (NAc; vSUB^{NAc}) shell, lateral hypothalamus (LH; vSUB^{LH}) and prefrontal cortex (PFC; vSUB^{PFC}) [16, 17]. These projections are mainly glutamatergic [18–22]. It is

well established that stimulation of the vHPC induces a release of dopamine (DA) in the NAc shell and medial PFC (mPFC) [23, 24], and extracellular DA levels within these regions fluctuate across the sleep–wake cycle [25]. Moreover, previous studies have demonstrated that NAc dopamine D1 receptor (D1R)-expressing neurons and NAc D2R-expressing neurons promote wakefulness and non-REM (NREM) sleep, respectively [26]. Considerable evidence indicates that the LH of the diencephalon is importantly involved in the circadian variability of the sleep–wake cycle. The orexin system in the LH is necessary for the stability of the arousal state, and specific orexin deficiency results in narcolepsy with cataplexy [27]. Melanin-concentrating hormone (MCH)-containing neurons, another important neuronal subtype in the LH, are most active during REM sleep, and stimulation of these neurons in sleep selectively promotes REM sleep [28]. Based on neuroanatomy and physiological evidence across species, the PFC is a key node in arousal circuitry, especially during the recovery from unconscious states such as general anesthesia [29]. In addition, the vSUB exhibits connections with the suprachiasmatic nucleus (SCN), which plays a crucial role in circadian rhythm regulation [30]. The SCN may provide a critical interface for the hippocampal inputs to influence general behavioral states and affect. Thus, we hypothesized that the vSUB could regulate arousal by forming synaptic contacts with several downstream regions.

To verify our hypothesis, we first employed fiber photometry and multichannel electrophysiological recordings to investigate

¹Department of Radiology, Zhongnan Hospital of Wuhan University, Wuhan University, Wuhan 430071, China. ²Department of Nuclear Medicine, Zhongnan Hospital of Wuhan University, Wuhan University, Wuhan 430071, China. ³Department of Pathology, Taikang Medical School (School of Basic Medical Sciences), Wuhan University, Wuhan 430071, China. ⁴Center for Pathology and Molecular Diagnostics, Zhongnan Hospital of Wuhan University, Wuhan University, Wuhan 430071, China. ⁵These authors contributed equally: Xue-Fen Zhang, Yi-Dan Li. ✉email: linlinbi2016@whu.edu.cn; xuhaibo@whu.edu.cn

Received: 30 November 2023 Revised: 20 April 2024 Accepted: 23 April 2024

Published online: 11 May 2024

the activity of vSUB neurons during the spontaneous sleep–wake cycle. Next, we examined the roles of vSUB and its neural circuits in wakefulness control and the necessity of DA signaling in this process. Collectively, our results provide several lines of evidence regarding vSUB glutamatergic neurons and circuit mechanisms for arousal in male mice.

MATERIALS AND METHODS

Mice

Male C57BL/6 mice (8–20 weeks), weighing 20–30 g, were purchased from Beijing Vital River Laboratory Animal Technology Co., Ltd. Mice were housed in cages with food and water ad libitum. Cages were maintained in a room with an appropriate temperature range of 20–24 °C and a relative humidity level of 40–60% under a 12 h light/12 h dark cycle (lights on at zeitgeber time 0 (ZT 0; 7:00)). For the entire study, a total of 180 mice were used. All experimental protocols for animal studies were approved by the Zhongnan Hospital of Wuhan University Experimental Animal Welfare and Ethics (ZN2021159).

Surgery

Mice were anesthetized with an intraperitoneal (i.p.) injection of 1% pentobarbital sodium (75 mg/kg) and placed on a stereotaxic frame (RWD, Shenzhen, China). A burr hole was made, and then the virus (50–100 nl) was delivered using Pump11 Elite Nanomite (70–4507, Harvard Apparatus, USA) via a glass micropipette opening ~20 µm attached to a 10 µl microsyringe. After an injection at a rate of 20 nl/min, the micropipette was left in place for 10 min and then slowly retracted. In chemogenetic, optogenetic, and fiber-photometry experiments, AAV2/9-CaMKIIa-hM3Dq-mCherry (titer: 5.3×10^{12} vector genomes (vg) ml⁻¹), AAV2/9-CaMKIIa-hM4Di-mCherry (titer: 2.9×10^{12} vg/ml), AAV2/9-CaMKIIa-ChR2-mCherry (titer: 3.7×10^{12} vg/ml), AAV2/9-CaMKIIa-mCherry (titer: 5.4×10^{12} vg/ml), or AAV2/9-CaMKIIa-GCaMP6f (titer: 2.0×10^{12} vg/ml) was injected into the vSUB (AP: -3.40 mm, ML: ±3.00 mm, DV: -4.65 mm). For chemogenetic activation of NAc-, LH-, or PFC-projecting vSUB glutamatergic neurons, Cre-expressing retrograde virus (AAV2/Retro-Syn-Cre, titer: 5.4×10^{12} vg/ml) was injected bilaterally into the NAc shell (AP: +1.30 mm; ML: ±0.50 mm; DV: -4.20 mm), LH (AP: -1.30 mm; ML: ±0.90 mm; DV: -4.90 mm), or PFC (AP: +1.90 mm; ML: ±0.40 mm; DV: -2.00 mm), and Cre-dependent recombinant AAV encoding hM3Dq (AAV2/9-CaMKIIa-DIO-hM3Dq-mCherry, titer: 5.0×10^{12} vg/ml) was injected into the vSUB. All of these AAVs were packaged by BrainVTA Technology (Wuhan, China). The coordinates used for viral injection were measured according to the atlas of the mouse brain (Franklin and Paxinos, Third Edition).

In fiber photometry and optogenetic experiments, optical fiber (fiber core: 200 µm, numerical aperture: 0.37, Inper, China) was implanted above the targeted nuclei 3–4 weeks after the virus injection. For multichannel electrophysiological recordings, an electrode array (Bio-Signal, Nanjing, China) using 16 nickel-cadmium wires was advanced into the vSUB. Signals were monitored in real time to gain a fine signal-to-noise ratio of spike activities. Reference and ground electrodes were fixed in the skull above the cerebellum. For local drug microinjection, a double guide cannula (0.34 mm, RWD) was implanted above the NAc (AP: +1.30 mm; ML: ±0.50 mm; DV: -3.70 mm), LH (AP: -1.30 mm; ML: ±0.90 mm; DV: -4.40 mm), or PFC (AP: +1.90 mm; ML: ±0.50 mm; DV: -1.50 mm) 3 weeks after virus injection.

All the mice were chronically implanted with electroencephalogram/electromyogram (EEG/EMG) electrodes for polysomnographic recordings 3–4 weeks after virus injection. Basically, the implants were comprised of 4 stainless-steel screws (1.0 mm diameter) with wire leads, two of which served as EEG electrodes (AP: +1.0 mm, ML: ±1.5 mm from the bregma), and the other two served as reference and ground (AP: +1.0 mm, ML: ±1.5 mm from the lambda), respectively. Besides, two multi-stranded PFA-coated stainless steel wires (793500, A-M System, USA) were placed bilaterally into the dorsal cervical neck muscles, serving as EMG electrodes. EEG and EMG electrodes were soldered into a headmount. Next, the whole assembly was covered with Super-Bond C&B and dental cement. The mice were kept individually and allowed to recover for at least 7 days after surgery.

Fiber photometry recordings and data analysis

The fiber photometry system (Thinkertech, Nanjing, China) was used to monitor neural activity by measuring Ca²⁺-dependent fluorescence. EEG/

EMG signals were also recorded at the same time (see below). In this system, the unique 405 nm channel was used as a reference channel to effectively remove movement noise, and a beam of 470 nm laser light excited GCaMP to detect changes in calcium signals. The laser power at the tip of the optical fiber was adjusted to 10–20 µW to minimize bleaching.

Analysis of the resulting signals was performed with custom-written MATLAB scripts. We derived the value of the photometry signal ($\Delta F/F$) by calculating $(F - F_0)/F_0$, where F_0 was the baseline fluorescence signal. For the sleep–wake analysis, we recorded data for 6–8 h per mouse. Each recording session lasted for 0.5 to 1 h ($n = 5$ mice; 1 mouse was excluded). For the state transition analyses, we identified the time points of state transition and aligned $\Delta F/F$ around these times (± 50 s).

In vivo multichannel electrophysiological recordings and firing rate analysis

Electrodes were connected to a 16-channel headstage kit (Bio-Signal, China). Signals were digitized at 30 kHz and obtained by Apollo II acquisition software (Bio-Signal, China). For sleep–wake analysis, data were collected during the light phase ($n = 3$ mice).

The spike sorting was processed using principal component analysis via Offline Sorter software (version 2.0, Plexon). The first two principal components on the two-dimensional plot of detected spike events were extracted and represented. The K-means method was used to cluster waveforms with similar principal components. The isolated cluster was considered to be recorded from a single neuron. Cross-correlation histograms were used to eliminate cross-channel artifacts. Spikes with inter-spike intervals < 1 ms were discarded. NeuroExplorer software (version 5.0) was used to produce firing rate rastergrams and histograms.

Polysomnographic recordings and analysis

In order to allow the animal's sleep patterns to adapt to the tether arrangement before collecting long-term waveforms, mice were kept individually in test cages and allowed to acclimate for 2 days after the preamplifier connected to the headmount. EEG/EMG signals were recorded under baseline (fiber photometry and electrophysiology studies) and different treatment conditions (chemogenetic and optogenetic manipulations).

The EEG/EMG signals were amplified, filtered (EEG: 0.3–30 Hz, EMG: 50–150 Hz), and then digitized at a sampling rate of 1 kHz using an 8-channel Medusa data acquisition system (Bio-Signal, China). Sleep–wake states were scored offline using Sirenia Sleep Pro software (Pinnacle, USA). All scoring was semiautomatic based on EEG and EMG waveforms in 4 s epochs. In general, most of the polygraphic recordings were automatically scored, and the remaining epochs were manually classified. The scoring was next examined visually and corrected manually when appropriate. The distinctions between vigilance states were based on previously described standard criteria [31–34]. The EEG power spectrum data were expressed as relative values to the total power of the same sleep–wake stage.

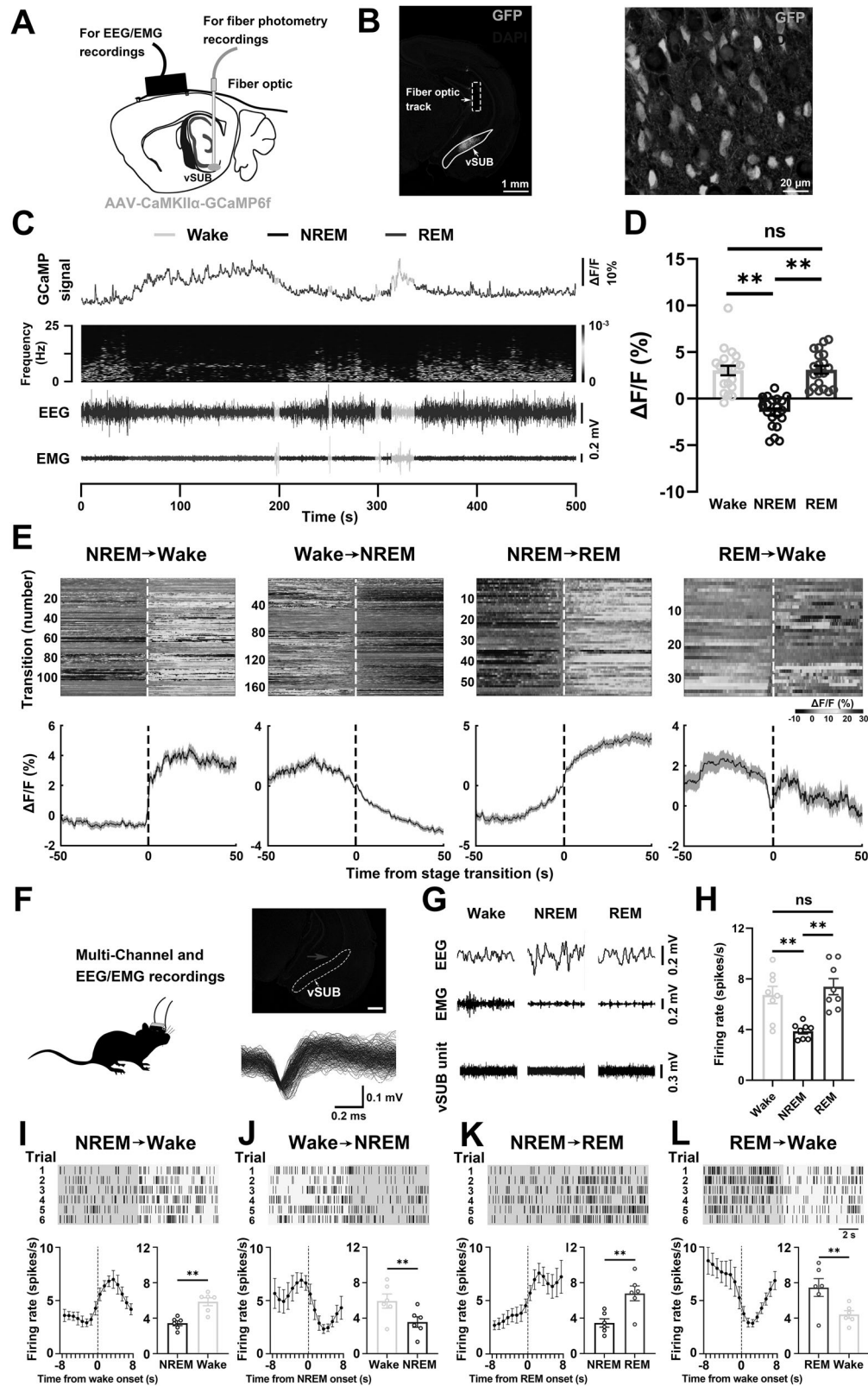
For sleep architecture analysis, wake and NREM sleep episodes were defined as lasting at least 1 min allowing an interruption of 4–16 s. Considering that REM episodes were generally shorter than wake and NREM episodes in mice, REM sleep episodes were defined as lasting at least 16 s allowing an interruption of 4–8 s as described in previous work [35].

Optogenetic stimulation

A total of 90 mice ($n = 47$ for ChR2 mice and $n = 43$ for mCherry mice; 7 mice were excluded) were used in optogenetic experiments. Before the testing day, the mouse was connected to an optical fiber patch cord (50 cm long, 200 µm diameter, Inper) with another side connected to a fiber rotary joint (Inper, China) to allow free movement. Another patch cord was connected from the joint to an intelligent photogenetic system (Thinkertech, China) that generated 473 nm blue light. The power of an optical signal passed through the fiber cable was calibrated to emit 8–12 mW at the tip. For acute photostimulation experiments, optical stimuli (10 ms pulses) were applied ~20 s after the onset of stable NREM or REM sleep epochs by detecting the online EEG/EMG display during the inactive period. For chronic photostimulation experiments, programmed light pulse trains (10 ms blue pulses at 10 Hz, with 4 s on/26 s off for 120 cycles) were used for 1 h from ZT 2 to ZT 3.

Pharmacological injections

In the DREADD experiments, a total of 82 mice (10 mice were excluded) were used. Clozapine-N-oxide (CNO, 4936, Tocris, USA) solution was freshly



prepared on each experimental day to achieve a final concentration of 0.05 mg/ml in 1% dimethyl sulfoxide (DMSO). Mice received an i.p. injection of either vehicle or CNO (1 mg/kg) at ZT 2 (hM3Dq and mCherry mice) or ZT 14 (hM4Di and mCherry mice) on 2 consecutive days. After

recordings, mice were killed 90 min after vehicle or CNO injection for further immunohistochemical staining.

In the chemogenetic pharmacological experiments, SCH-23390 hydrochloride (D1R antagonist, 600 ng/0.3 μ l; MedChemExpress; USA) or

Fig. 1 Neural activity of vSUB glutamatergic neurons across spontaneous sleep–wake cycle. **A** Schematic diagram of in vivo fiber photometry and EEG/EMG recordings. **B** Representative images of the vSUB GCaMP6f-expressing brain section immunostained for DAPI, showing viral expression and the position of a fiber optic above the vSUB. **C** Representative fluorescence trace, EEG power spectrogram, and EEG/EMG traces across the spontaneous sleep–wake cycle. The color scale indicates the power spectral density (mV^2/Hz). **D** Fluorescence during wakefulness, NREM sleep, and REM sleep ($n = 4$ mice, 5 sessions per mouse; one-way ANOVA, $F_{2,38} = 34.35$, $P < 0.001$; followed by Tukey's post hoc tests, P (wake vs NREM) < 0.001 , P (wake vs REM) = 0.991, P (NREM vs REM) < 0.001). **E** Fluorescence aligned to state transitions. Top: Individual transitions with color-coded fluorescence intensity (NREM-to-wake, $n = 118$; wake-to-NREM, $n = 174$; NREM-to-REM, $n = 56$; REM-to-wake, $n = 35$). Bottom: Average responses from all the transitions expressed as mean (blue trace) \pm SEM (light blue shading). **F** Schematic configuration of in vivo multichannel electrophysiological and EEG/EMG recordings. Top: A brain slice from a mouse with electrodes implanted in the vSUB. The red arrow indicates the electrode track. Scale bar: 500 μm . Bottom: Waveforms from a recorded vSUB neuron. **G** EEG/EMG and vSUB unit traces during wakefulness, NREM sleep, and REM sleep. **H** Average firing rate of vSUB neurons during each state ($n = 8$ cells from 3 mice, one-way repeated measures (RM) ANOVA, $F_{2,14} = 13.53$, $P = 0.001$; followed by LSD post hoc tests, P (wake vs NREM) = 0.006, P (NREM vs REM) = 0.001, P (REM vs wake) = 0.430). Firing rate of vSUB neurons during state transitions: NREM-to-wake (**I**), wake-to-NREM (**J**), NREM-to-REM (**K**), and REM-to-wake transitions (**L**). Top: Example rastergrams of vSUB neurons during six trials of different state transitions. Bottom left: Average firing rate during the state-transition period. Bottom right: Average firing rate within 8 s before and after state transitions (paired t test, P (NREM-to-wake) < 0.001 , P (wake-to-NREM) = 0.009, P (NREM-to-REM) = 0.002, P (REM-to-wake) = 0.005). Data are represented as mean \pm SEM (** $P < 0.01$, ns: not significant).

raclopride (D2/D3R antagonist, 3 $\mu\text{g}/0.3 \mu\text{l}$; MedChemExpress; USA) was delivered into the NAC, LH, or PFC via an injection cannula that extended 0.5 mm beyond the tip of the guide cannula after CNO (1 mg/kg, i.p.) administration.

Behavioral tests

Open field (OF) test. Mice were introduced into the center of a $50 \times 50 \times 50 \text{ cm}$ white box. Exploratory behaviors were recorded for 5 min with a video-tracking system (VisuTrack, Shanghai, China). The locomotion distance and the time spent in the center of the arena ($25 \times 25 \text{ cm}$) were measured.

Elevated plus maze (EPM) test. Mice were placed in the central region of an elevated (50 cm) plus-shaped track and oriented towards an open arm. The apparatus consisted of a central region ($10 \times 10 \text{ cm}$), two open arms ($50 \times 10 \text{ cm}$), and two closed arms ($50 \times 10 \times 40 \text{ cm}$). The time spent in open arms and the number of entries onto open arms were recorded during the 5 min test.

Real-time place preference (RTPP) test. A custom-made two-chamber apparatus ($30 \times 30 \times 30 \text{ cm}$ for each chamber) was used. On the first day, mice were allowed to freely explore between the two chambers without optogenetic stimulation for 15 min. On the second day, mice received optogenetic stimulation (10 Hz) while entering the test chamber. The laser was turned off when the mice returned to the other side. Results were presented as a percentage of time spent on the stimulation side during the test.

Immunohistochemistry. Mice were deeply anesthetized with chloral hydrate (200 mg/kg) and urethane (1000 mg/kg) and then perfused intracardially through the left ventricle with PBS, followed by 4% paraformaldehyde (PFA). Brains were removed, postfixed for 12 h in 4% PFA, and then stored in a sucrose solution (30% sucrose in PBS) at 4°C until they sank. Next, the brains were coronally sectioned at $40 \mu\text{m}$ on a freezing microtome (CM1900, Leica, Germany) at -20°C .

For immunostaining, the floating sections were incubated in blocking buffer (P0260, Beyotime, China) for 1 h at room temperature (RT) and then incubated with primary antibodies diluted in primary antibody dilution buffer (P0262, Beyotime, China) at 4°C overnight. The following primary antibodies were used: rabbit anti-c-Fos (1:1000, 2250, CST), mouse anti-c-Fos (1:300, ab302667, Abcam), rabbit anti-orexin-B (1:500, ab255293, Abcam), rabbit anti-MCH (1:500, ab274415, Abcam). The next day, sections were washed with PBS and incubated with secondary antibodies (donkey anti-rabbit Alexa 488, 1:1000, A21206, Invitrogen; goat anti-mouse Alexa 647, 1:1000, A21235, Invitrogen) for 2 h at RT. After rinsing, the sections were immersed in DAPI for 15 min at RT. Finally, the sections were mounted on glass slides, dried, and coverslipped.

To verify the location of the fiber optic, electrode, and cannula, mouse brains were fixed and prepared as described above. The whole mouse brain was sectioned at $40 \mu\text{m}$. Sections containing the tracks were washed three times in PBS, then immersed in DAPI for 15 min at RT. Finally, the sections were mounted on slides and coverslipped. High-resolution fluorescence

images were obtained on a confocal microscope (SP8, Leica). Digital images were processed using LAS X FLIM FCS Offline and Adobe Photoshop 2020 software to minimally adjust brightness and contrast.

Statistical analysis

All data were presented as mean \pm standard error of the mean (SEM). Statistical significance between the two groups was assessed using the paired or unpaired two-tailed student's t test. One-way or two-way analyses of variance (ANOVA) were used for comparisons of three or more groups. $P < 0.05$ was considered statistically significant. Post hoc significance values were set as * $P < 0.05$, ** $P < 0.01$. The data were analyzed using SPSS statistical software. Figures were drawn and adjusted using GraphPad Prism 9.0 and Adobe Photoshop 2020.

RESULTS

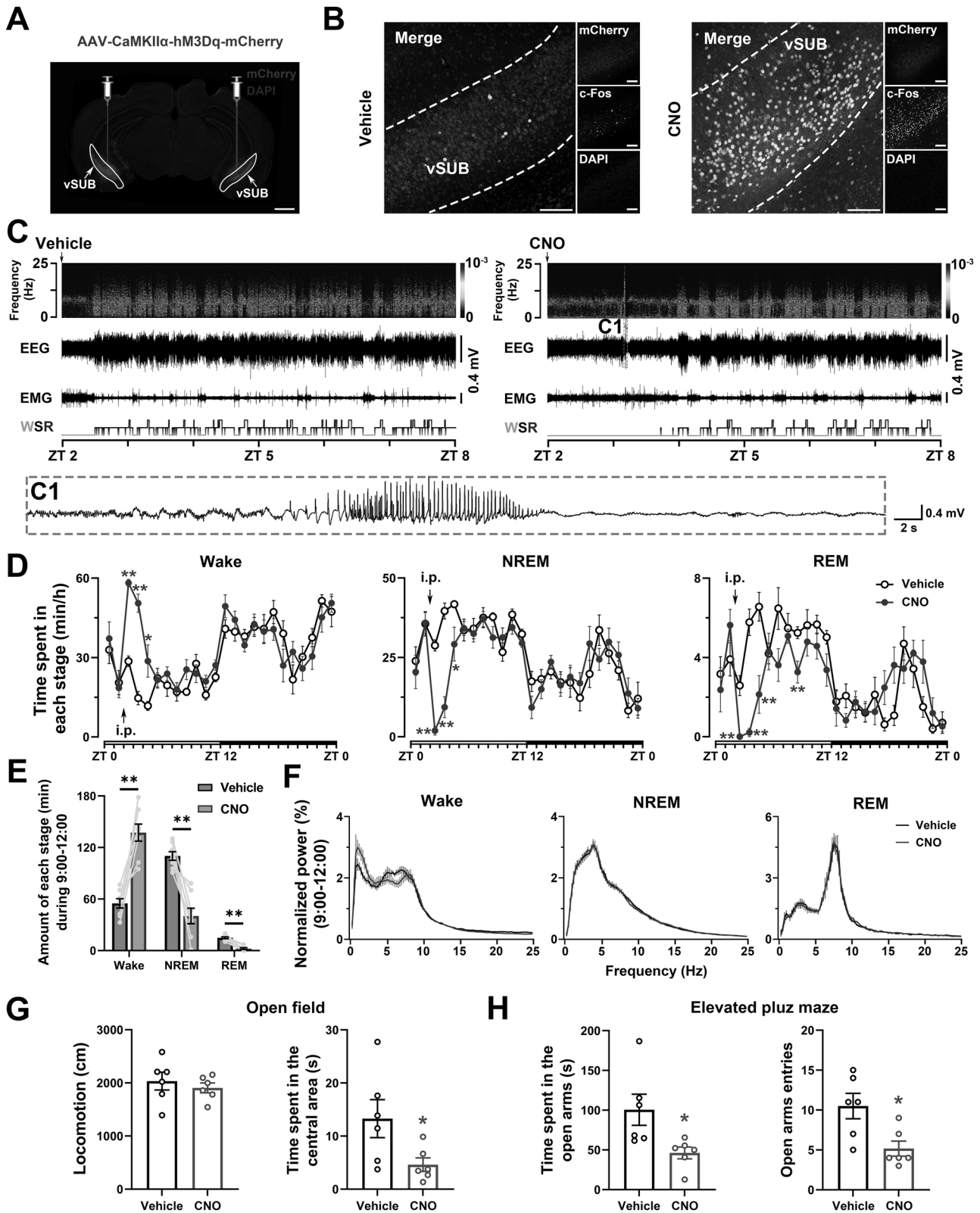
The activity of vSUB glutamatergic neurons increases during wakefulness

To assess the physiological real-time activity of vSUB glutamatergic neurons across the spontaneous sleep–wake cycle, we recorded the calcium activity of vSUB glutamatergic neurons via fiber photometry. The AAV encoding the fluorescent calcium indicator GCaMP6f under the control of the CaMKIIa promoter was injected into the vSUB. After 3–4 weeks of virus injection, we implanted a fiber optic with its tip above vSUB to record calcium activity. EEG/EMG electrodes were simultaneously inserted into the cortical surface and neck muscles to define sleep–wake states (Fig. 1A). GCaMP-positive cell bodies were observed in the vSUB (Fig. 1B). When comparing the fluorescence signals of vSUB glutamatergic neurons across sleep–wake states, we observed significantly higher fluorescence signals during wakefulness and REM sleep than during NREM sleep (Fig. 1C, D). Notably, a dramatic increase in GCaMP activity of vSUB glutamatergic neurons was found during NREM-to-wake and NREM-to-REM transitions, whereas decreased GCaMP activity occurred during wake-to-NREM and REM-to-wake transitions (Fig. 1E).

We next performed in vivo multichannel electrophysiological recordings to monitor the firing rate of individual vSUB neurons in freely behaving mice (Fig. 1F). vSUB neurons exhibited a higher firing rate during wakefulness and REM sleep than during NREM sleep (Fig. 1G–L). At the transitions from NREM sleep to wakefulness, the mean firing rate reached $6.98 \pm 0.84 \text{ Hz}$ in the fourth second after behavioral arousal (Fig. 1I). Collectively, these findings suggest that the vSUB glutamatergic neurons may play an important role in sleep–wake control.

Chemogenetic or optogenetic activation of vSUB glutamatergic neurons significantly increases wakefulness and anxiety-like behaviors

To explore the role of vSUB glutamatergic neurons in sleep–wake regulation and anxiety-like behaviors, we bilaterally injected AAV-



CaMKII α -hM3Dq-mCherry into the vSUB of wild-type mice (vSUB-hM3Dq mice). After 3–4 weeks, the hM3Dq-expressing vSUB neurons were potentially activated by systemic CNO administration (Fig. 2A, B). To monitor sleep–wake behavior, mice received i.p.

injections of either vehicle or CNO (1 mg/kg) at ZT 2. In vSUB-hM3Dq mice, CNO administration significantly increased wakefulness lasting approximately 3 h and concomitantly decreased both NREM and REM sleep, as compared with vehicle control

Fig. 2 Chemogenetic activation of vSUB glutamatergic neurons increases wakefulness and anxiety-like behaviors. **A** Representative image of virus injection at the vSUB. Scale bar: 1 mm. **B** Representative images of mCherry/c-Fos/DAPI immunofluorescence in vSUB after vehicle or CNO treatment. Scale bar: 100 μ m. **C** Typical examples of EEG power spectrum, EEG/EMG traces, and hypnograms over 6 h after vehicle or CNO injection at ZT 2 in an hM3Dq mouse. **C1**: EEG recordings during a seizure after CNO injection. Each letter of WSR represents wakefulness, SWS (also known as NREM sleep), and REM sleep, respectively. **D** Time-course changes in wakefulness, NREM sleep, and REM sleep after vehicle or CNO administration ($n = 8$, two-way RM ANOVA between compound injected and time; Wake: $F_{1,14} = 3.99$, $P < 0.001$; NREM: $F_{1,14} = 3.77$, $P < 0.001$; REM: $F_{1,14} = 4.05$, $P < 0.001$, followed by Sidak's post hoc tests). **E** The total time spent in each stage during the 3 h after vehicle or CNO injection ($n = 8$, paired t test; Wake: $t_{14} = 6.26$, $P < 0.001$; NREM: $t_{14} = 5.76$, $P = 0.001$; REM: $t_{14} = 8.38$, $P < 0.001$). **F** EEG power density of wakefulness, NREM sleep, and REM sleep for 3 h after vehicle or CNO administration ($n = 6$; two-way ANOVA; Wake: $P = 0.003$). **G** Locomotion (left) and time spent in the central area (right) in the OF test ($n = 6$, paired t test; left: $t_{10} = 0.99$, $P = 0.369$; right: $t_{10} = 2.81$, $P = 0.037$). **H** Time spent in the open arms (left) and the open arms entries (right) in the EPM test ($n = 6$, paired t test; left: $t_{10} = 2.60$, $P = 0.048$; right: $t_{10} = 3.32$, $P = 0.021$). Data are represented as mean \pm SEM (* $P < 0.05$, ** $P < 0.01$).

(Fig. 2C–E). However, CNO did not affect the time spent in each stage across the 24-h sleep–wake cycle of mice transduced with the control virus (AAV-CaMKII α -mCherry, mCherry mice; Supplementary Fig. 1). Intriguingly, we found epileptiform activity on EEG 40–70 min after CNO administration in vSUB-hM3Dq mice, generally lasting a few tens of seconds (Fig. 2C1). Compared to the vehicle group, CNO treatment increased the EEG low delta power (0.49–1.98 Hz) and decreased theta power (6.17–6.92 Hz) during the 3 h post-injection period. While there was no significant difference in the EEG power density during NREM and REM sleep (Fig. 2F). To investigate the potential effects of CNO on sleep, we first analyzed the first 3 h and 6 h observation time window in mCherry mice after vehicle or CNO injection at ZT 2. We found no significant main effect of the treatment condition on the proportion of the recording time spent in wakefulness, NREM sleep, and REM sleep, but the amount of REM sleep relative to the total sleep time (TST) decreased within the first 3 h following drug administration (Supplementary Fig. 2). Moreover, CNO did not alter sleep architecture in mCherry mice (Supplementary Fig. 3).

Next, we used optogenetic methods that allow millisecond-scale control of neuronal activity to study the effects of vSUB glutamatergic neurons on wakefulness initiation and maintenance. We injected AAV expressing channelrhodopsin-2 (AAV-CaMKII α -ChR2-mCherry, 'ChR2' hereafter) or control virus (AAV-CaMKII α -mCherry) into the vSUB. After 3–4 weeks of virus injection, we implanted the mice with a fiber optic probe above the vSUB and with EEG/EMG electrodes (Supplementary Fig. 4A, B). Phasic 10-Hz stimulation (10 ms) of vSUB glutamatergic neurons induced a rapid transition from NREM-to-wake (latency: 3.74 ± 0.43 s) and REM-to-wake (latency: 6.12 ± 0.58 s) in ChR2 mice but not in mCherry mice (Supplementary Fig. 4C–E, Supplementary Fig. 5). To determine whether vSUB glutamatergic neurons also contributed to the maintenance of wakefulness, blue light pulse trains (10 ms per pulse, 10 Hz for 4 s/30 s) were given for 1 h during ZT 2 to ZT 3. Sustained activation of vSUB glutamatergic neurons via chronic optical stimulation significantly promoted wakefulness and suppressed both NREM and REM sleep in ChR2 but not in mCherry mice. During the following light phase (ZT 3 to ZT 12), there was no significant difference between ChR2 and mCherry mice in sleep–wake amount (Supplementary Fig. 4F). These findings demonstrate that activation of vSUB glutamatergic neurons potently enhances both the initiation and maintenance of wakefulness.

Previous studies have demonstrated that the neural pathways of vSUB are necessary for normal anxiety-like and avoidance behaviors [3, 36]. To explore whether activation of vSUB glutamatergic neurons could promote anxiety-like or avoidance behaviors, we explored behaviors after chemogenetic (Fig. 2G, H) or optogenetic (Supplementary Fig. 4G, H, I) activation of vSUB glutamatergic neurons. In hM3Dq and ChR2 mice, activation of vSUB glutamatergic neurons decreased the time spent in the central area in the OF test, as well as the time spent in the open

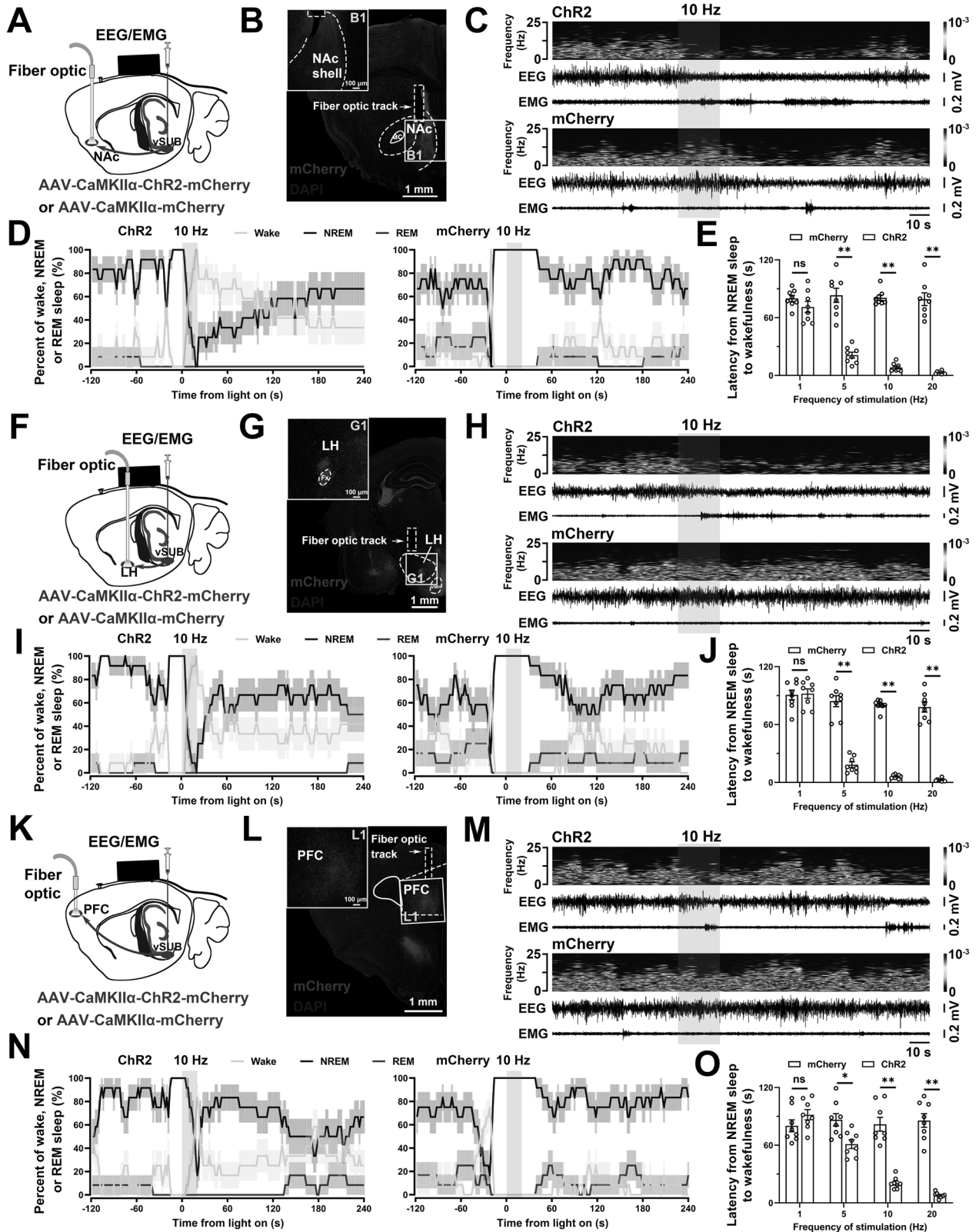
arms and the number of entries onto the open arms in the EPM test. In contrast, there were no changes in locomotion activity in the OF test between the experimental group and control group. In the RTPP test, we found that optogenetically stimulated ChR2 mice spent a decreased proportion of their time in the stimulation-paired zone compared with baseline. Taken together, increased arousal induced by activating vSUB glutamatergic neurons is associated with aversive and anxiety-like behaviors.

The vSUB glutamatergic neurons promote wakefulness via NAc, LH, and PFC circuits

To elucidate the neuronal circuits mediating the wake-promoting effect of vSUB glutamatergic neurons, AAV-CaMKII α -ChR2-mCherry was injected into the vSUB, and the optic fiber was implanted above the axon terminals in the NAc (Fig. 3A), LH (Fig. 3F), or PFC (Fig. 3K), based on the vSUB projection neurons [17] (Fig. 3B, G, L). Phasic 10-Hz stimulation of the vSUB glutamatergic terminals in the NAc (Fig. 3C, D; latency: 8.28 ± 1.48 s) or LH (Fig. 3 H, I; latency: 6.13 ± 0.67 s) strongly and consistently promoted waking from NREM sleep in ChR2 mice but not in mCherry mice. In contrast, photostimulation at 10 Hz of the PFC projections in vSUB-ChR2 mice also induced transitions from NREM-to-wake (latency: 20.60 ± 2.13 s), but the time spent in wakefulness rapidly decreased after stimulation (Fig. 3M, N). Moreover, selective optogenetic activation of the vSUB glutamatergic terminals in the NAc (Fig. 3E), LH (Fig. 3J), or PFC (Fig. 3O) shortened the NREM-to-wake latencies in a stimulation frequency-dependent manner.

To further investigate the role of the vSUB^{Glu}-NAc, vSUB^{Glu}-LH, and vSUB^{Glu}-PFC pathways in mediating the wakefulness-maintaining effects, we used loop-specific chemogenetics to selectively activate NAc-, LH-, or PFC-projecting vSUB glutamatergic neurons. We injected retrograde AAV encoding Cre (AAV_{retro}-Syn-Cre) into bilateral downstream targets while injecting a Cre-dependent AAV encoding hM3Dq (AAV-CaMKII α -DIO-hM3Dq-mCherry) into the vSUB (Supplementary Fig. 6A, D, G). Immunohistochemistry showed that activation of the NAc-, LH-, or PFC-projecting vSUB glutamatergic neurons (mCherry+) upregulated c-Fos expression after CNO administration (Supplementary Fig. 6B, E, H). Compared to vehicle control, CNO injection in vSUB^{NAc}-hM3Dq, vSUB^{LH}-hM3Dq, or vSUB^{PFC}-hM3Dq mice significantly increased wakefulness with decreases in NREM and REM sleep during the 2–3 h following administration (Supplementary Fig. 6C, F, I). These results suggest that vSUB modulates arousal through NAc, LH, and PFC.

Moreover, to find the potential pathway of the vSUB^{Glu}-LH circuit in regulating arousal, we double-labeled orexin/c-Fos or MCH/c-Fos in vSUB^{LH}-hM3Dq mice. The CNO treatment increased c-Fos expression in LH orexin neurons (Supplementary Fig. 7A, B) but not in MCH neurons (Supplementary Fig. 7C, D), indicating that vSUB glutamatergic neurons may also regulate arousal through the orexin neurons in the LH.



Local blockade of dopamine receptors abolishes wake-promoting effects induced by activation of vSUB pathways
 Previous studies reported that glutamatergic afferents from the vSUB regulate the activity of DAergic axons in the NAc and PFC

[24, 37]. To further investigate the role of DA signaling in sleep–wake regulation, either the D1R antagonist SCH-23390 or the D2/D3R antagonist raclopride was microinjected into the NAc, LH, or PFC after chemogenetic activation of NAc-, LH-, or PFC-projecting

Fig. 3 The vSUB glutamatergic neurons control arousal through the NAc, LH, and PFC pathways. Schematic diagram of optogenetic stimulation of vSUB glutamatergic terminals in the NAc (A), LH (F), or PFC (K) together with EEG/EMG recordings. Sections stained for DAPI showing Chr2-mCherry-positive terminals in the NAc (B), LH (G), or PFC (L). Representative EEG power spectrum and EEG/EMG traces around 10 Hz stimulation of vSUB glutamatergic terminals in the NAc (C), LH (H), or PFC (M) during NREM sleep in a Chr2 mouse and a mCherry mouse. The blue column indicates the photostimulation period. Percentages of wakefulness, NREM and REM sleep after acute photostimulation of vSUB glutamatergic terminals in the NAc (D), LH (I), or PFC (N) during NREM sleep in Chr2 and mCherry mice (12 trials per group). Mean latencies of wake transitions during NREM sleep after acute photostimulation of vSUB glutamatergic terminals in the NAc (E, $n = 8$ per group, unpaired t test; 1 Hz: $t_{1,4} = 1.35$, $P = 0.200$; 5 Hz: $t_{1,4} = 7.81$, $P < 0.001$; 10 Hz: $t_{1,4} = 22.93$, $P < 0.001$; 20 Hz: $t_{1,4} = 11.61$, $P < 0.001$), LH (J, $n = 8$ per group; 1 Hz: $t_{1,4} = 0.19$, $P = 0.849$; 5 Hz: $t_{1,4} = 10.33$, $P < 0.001$; 10 Hz: $t_{1,4} = 36.18$, $P < 0.001$; 20 Hz: $t_{1,4} = 14.57$, $P < 0.001$), or PFC (O, $n = 8$ per group; 1 Hz: $t_{1,4} = 1.41$, $P = 0.179$; 5 Hz: $t_{1,4} = 3.21$, $P = 0.006$; 10 Hz: $t_{1,4} = 8.20$, $P < 0.001$; 20 Hz: $t_{1,4} = 10.95$, $P < 0.001$) at different frequencies in Chr2 and mCherry mice. Data are represented as mean \pm SEM (* $P < 0.05$, ** $P < 0.01$, ns: not significant).

vSUB glutamatergic neurons, respectively (Fig. 4A). The protocol for virus injection was the same as the loop-specific chemogenetic experiments in Supplementary Fig. 6. After 3–4 weeks of virus injection, a double-guide cannula was implanted above the NAc, LH, or PFC (Fig. 4B, C). In consistent with the results of Supplementary Fig. 6, chemogenetic activation of NAc-, LH-, or PFC-projecting vSUB glutamatergic neurons significantly increased wakefulness in vSUB^{NAc}-hM3Dq, vSUB^{LH}-hM3Dq and vSUB^{PFC}-hM3Dq mice, respectively (Supplementary Fig. 8). However, this wake-promoting effect was blocked by dopamine receptor antagonists, especially in vSUB^{NAc}-hM3Dq and vSUB^{PFC}-hM3Dq mice (Fig. 4B–G), indicating that dopamine signaling has a key role in promoting wakefulness through vSUB neural pathways.

The vSUB glutamatergic neurons are necessary for wakefulness

To examine whether the activity of vSUB glutamatergic neurons was essential for sustaining arousal, we specifically injected the AAV-CaMKII α -hM4Di-mCherry ('hM4Di' hereafter) into the vSUB (Fig. 5A). Immunohistochemistry showed that injection of the DREADD actuator CNO decreased c-Fos expression within hM4Di-expressing neurons in the vSUB (Fig. 5B). Either vehicle or CNO (1 mg/kg) was injected i.p. at ZT 14, when mice usually had a high level of spontaneous wakefulness. In hM4Di mice, CNO treatment significantly increased NREM sleep, which is characterized by high-amplitude, low-frequency EEG activity and low EMG activity, accompanied by a decrease in wakefulness during the 4 h following administration, as compared with vehicle control (Fig. 5C, D). For the total amount of time spent in wakefulness, NREM and REM sleep during the 4 h post-injection period, CNO administration to hM4Di mice significantly reduced wakefulness (vehicle: 171.78 ± 9.64 min; CNO: 107.19 ± 5.47 min) and increased NREM sleep (vehicle: 64.54 ± 8.94 min; CNO: 124.24 ± 5.47 min) and REM sleep (vehicle: 3.69 ± 1.21 min; CNO: 8.57 ± 1.01 min), as compared with vehicle control (Fig. 5E). In addition, the EEG power spectrum during NREM and REM sleep, induced by inhibition of vSUB glutamatergic neurons, was similar to the spectrum displayed during spontaneous sleep (Fig. 5F). Collectively, these results indicate that the vSUB glutamatergic neurons are essential for the maintenance of wakefulness.

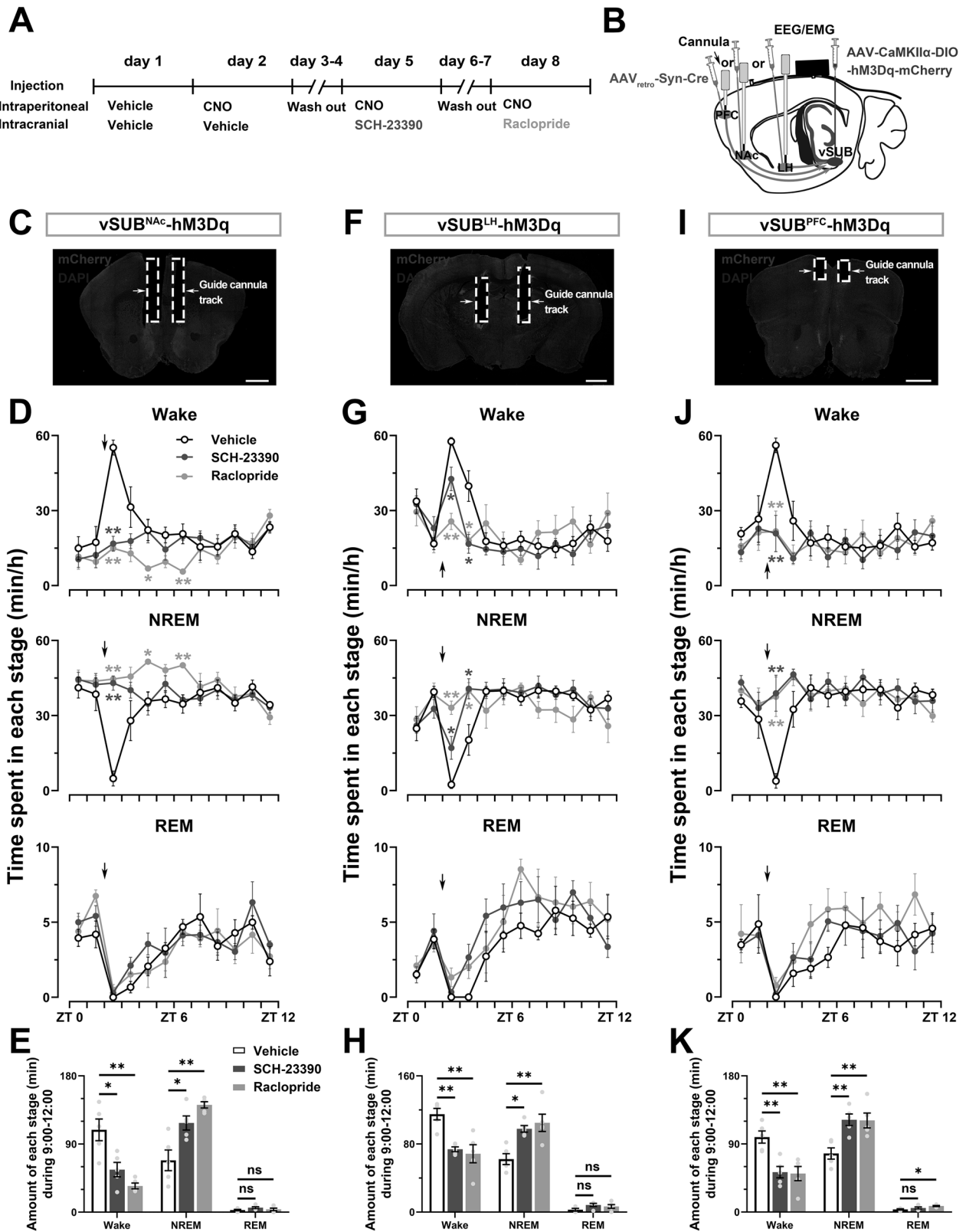
DISCUSSION

The vSUB affects motivation-related behaviors, including reward, food intake, learning, and memory [5, 10, 22]. These behaviors are crucial for survival, and animals will exhibit a high level of wakefulness to perform these behaviors. To uncover the role of vSUB glutamatergic neurons in sleep–wake regulation, we first revealed state-dependent alteration in neuronal activity of vSUB glutamatergic neurons, identifying an increase in neuronal activity during wakefulness. Next, we proved that vSUB glutamatergic neurons were sufficient and necessary for sleep–wake regulation.

Furthermore, we identified several circuits through which vSUB glutamatergic neurons regulated arousal. We demonstrated that activation of vSUB^{Glu}-NAc, vSUB^{Glu}-LH, or vSUB^{Glu}-PFC pathway promoted wakefulness and suppressed sleep. Finally, DA signaling was found to be necessary for the wake-promoting effect of the vSUB^{Glu}-NAc and vSUB^{Glu}-PFC pathways. Taken together, our findings identify a novel region and neural circuits in sleep–wake regulation.

Considerable evidence suggests that manipulation of the vHPC itself or its inputs and cortical outputs can directly impact anxiety-related behaviors [2, 38–44], including anxiety-like avoidance behaviors [3]. Using magnetoencephalography in humans, an anxious state has been shown to correlate with theta rhythm in the anterior hippocampus [45], a region which corresponds to vHPC in rodents [2]. Furthermore, lesions [46] and optogenetic inhibition [43] of the vHPC are anxiolytic. In agreement, we found that activation of the vSUB glutamatergic neurons increased anxiety-like behaviors and avoidance behaviors. Given the role of vSUB glutamatergic neurons in regulating wakefulness and anxiety-like behaviors, one explanation is that activation of these neurons induces behavioral arousal associated with anxiety, but detailed functional circuit mapping deserves further study.

The LH is a heterogeneous brain region of the hypothalamus, and its resident cell populations have been implicated in the regulation of many physiological processes, including sleep–wake control, feeding behavior, and energy metabolism [47]. While both LH MCH and orexin neurons function as sensors of the internal metabolic environment, their roles in regulating sleep and wakefulness are actually opposing. Orexin neurons are wake-active, wake-promoting, and fire maximally during wakefulness and mostly silent during NREM and REM sleep [48]. On the contrary, activation of the MCH neurons promotes REM sleep but not NREM sleep [49, 50]. Anatomic studies have showed that pyramidal neurons in field vCA1 and vSUB are a major source of direct and exclusively ipsilateral input to the LH, especially the dorsal perifornical LH [51]. The dorsal perifornical LH also has abundant expression of the neuropeptide orexin [52]. Previous findings revealed novel neurobiological connections with appetite-associated vHPC neurons engaging in LH orexin signaling. The heightened responsiveness to external food-related cues following vHPC ghrelin signaling may be mediated by increased arousal, as well as potential circadian changes [22]. In agreement, our study found c-Fos co-expression with orexin neurons but not MCH neurons in the LH. These findings reveal that the vSUB^{Glu}-LH circuit may control arousal partially by activating LH orexin neurons. Moreover, DA receptor antagonists, especially D2R antagonist, blocked the wakefulness induced by activation of LH-projecting vSUB glutamatergic neurons. Pharmacological or chemogenetic stimulation of D2R-expressing cells in the LH and the zona incerta activates the sympathetic nervous system and ultimately leads to the increase of UCP1, brown adipose tissue temperature and energy



expenditure [53], which is closely related to the circadian timing system. Additional experiments are needed to determine the role of DA signaling in the wake-promoting effect of the vSUB^{Glu}-LH circuit.

The vSUB provides the most prominent glutamatergic input to the medial NAC shell [20], which has multiple D1R-expressing medium spiny neurons (MSNs), and these projections overlap with DAergic inputs from the ventral tegmental area (VTA) [54].

Fig. 4 Local blockade of dopamine receptors abolishes wake-promoting effects induced by activation of vSUB pathways. **A** Schematic of the experimental design. **B** A diagram illustrating the locations of virus injection, the cannula used for local drug microinjection, and EEG/EMG recordings. The example slice stained for DAPI showing the location of the double guide cannula above the NAc (**C**), LH (**F**), or PFC (**I**). Scale bar: 1 mm. Effects of local infusion after chemogenetic activation of NAc- (**D**, $n = 5$, two-way RM ANOVA between local injection drug and time; interaction: Wake: $F_{2,12} = 4.27$, $P < 0.001$; NREM: $F_{2,12} = 5.28$, $P < 0.001$; REM: $F_{2,12} = 0.87$, $P = 0.629$, followed by Sidak's post hoc tests), LH- (**G**, $n = 5$; interaction: Wake: $F_{2,12} = 2.79$, $P < 0.001$; NREM: $F_{2,12} = 3.35$, $P < 0.001$; REM: $F_{2,12} = 0.88$, $P = 0.626$), or PFC-projecting (**J**, $n = 5$; interaction: Wake: $F_{2,12} = 1.78$, $P = 0.025$; NREM: $F_{2,12} = 2.10$, $P = 0.005$; REM: $F_{2,12} = 0.64$, $P = 0.889$) vSUB glutamatergic neurons on the time-course changes in wakefulness, NREM sleep, and REM sleep. Red star: vehicle vs SCH-23390; blue star: vehicle vs raclopride. Arrows indicate the time point of the compound infusion. The total amount of time spent in each stage during the 3 h after vehicle or CNO injection in vSUB^{NAc}-hM3Dq (**E**, $n = 5$; one-way ANOVA; Wake: $F_{2,12} = 14.08$, $P = 0.001$; NREM: $F_{2,12} = 14.39$, $P = 0.001$; REM: $F_{2,12} = 1.55$, $P = 0.253$, followed by Bonferroni's post hoc tests), vSUB^{LH}-hM3Dq (**H**, $n = 5$; Wake: $F_{2,12} = 11.82$, $P = 0.001$; NREM: $F_{2,12} = 9.92$, $P = 0.003$; REM: $F_{2,12} = 2.39$, $P = 0.134$), or vSUB^{PFC}-hM3Dq mice (**K**, $n = 5$; Wake: $F_{2,12} = 10.69$, $P = 0.002$; NREM: $F_{2,12} = 9.29$, $P = 0.004$; REM: $F_{2,12} = 5.75$, $P = 0.018$). Data are represented as mean \pm SEM (* $P < 0.05$, ** $P < 0.01$, ns: not significant).

Previous studies found that NAc D1R-expressing neurons promote wakefulness by disinhibiting DA neurons of VTA [26], and VTA DAergic neurons modulate arousal mainly mediated by NAc projections [55]. In our study, the wakefulness induced by activation of NAc-projecting vSUB glutamatergic neurons was completely blocked by DA receptor antagonists. Therefore, it is conceivable that the vSUB drive of NAc neurons is potently modulated by the DA system. The vSUB modulates DA efflux in the NAc through at least two distinct mechanisms by numerous studies. First, the vSUB may increase the excitability of DA neurons in the VTA via a polysynaptic pathway through the ventral pallidum (VP) [56, 57]. Second, vSUB stimulation can also evoke direct presynaptic modulation of DA release by the action of glutamate on DA varicosities in the NAc [19]. Moreover, D1R- and D2R-expressing neurons in the NAc play opposite roles in sleep-wake control. Collectively, the NAc D1R-expressing neurons promote arousal, and the D2R-expressing neurons promote NREM sleep [26]. However, pretreatment with the D2/D3R antagonist raclopride completely abolishes the increased wakefulness evoked by VTA activation, whereas the D1R antagonist SCH-23390 does not [58]. It can be speculated from these studies that D1Rs have awakening effects, while D2Rs exhibit biphasic effects. Pharmacological experiments are also affected by a variety of factors, such as the routes of drug administration and the doses administered. Taken together, previous studies and our present findings elucidate a potential pathway of the vSUB-NAc-VP-VTA or vSUB-NAc-VTA circuit in modulating arousal.

The PFC has extensive reciprocal connections to wake-promoting centers in the brainstem and diencephalon [59, 60], and hence is in a unique position to modulate and control the level of consciousness. Related electrophysiological and anatomical studies indicate that pyramidal neurons in the mPFC send excitatory glutamatergic projections to the VTA DAergic neurons [61]. More importantly, DA is essential for the cognitive control functions of the PFC [62]. Our data confirms that vSUB potently modulates DA efflux in the PFC and has a specific role in sleep-wake regulation. Further studies will be required to determine the involvement of multisynaptic pathways and other neural circuits in sleep-wake regulation of vSUB glutamatergic neurons.

In this study, we focused on the role of vSUB glutamatergic neurons in wakefulness regulation. Interestingly, we found the neural activity of vSUB glutamatergic neurons was also increased during NREM-to-REM transitions, while neither optogenetic nor chemogenetic activation of vSUB glutamatergic neurons had a significant effect on REM sleep. This is consistent with previous findings [26, 63–65] and has not yet been better explained. In addition, vSUB sends extensive monosynaptic projections to crucial regions implicated in regulation of both wake and REM sleep, including the NAc, basal forebrain, and laterodorsal

tegmental nucleus [30]. We suspect that a subset of vSUB glutamatergic neurons project directly to the REM-related neurons, which need further investigation.

Typically, i.p. injections of CNO are used for DREADD experiments, and it is widely thought that CNO does not affect sleep [26, 66]. However, a recent study [35] found that CNO suppresses REM sleep and affects sleep architecture. We found that the amount of REM sleep relative to the TST decreased within the first 3 h following CNO injection, suggesting that the effects of CNO on sleep could arise from backmetabolism to clozapine or binding to endogenous neurotransmitter receptors. But we did not detect any alteration in sleep architecture. In chemogenetic activation experiments, although the decrease in REM sleep occurs primarily with an increase in wakefulness, we cannot exclude the effects of CNO on sleep.

The SUB is thought to be essential in the initiation and propagation of seizures in epilepsy [67]. Here, we found CNO administration triggered cortical hyperexcitability and seizure-like discharges in vSUB-hM3Dq mice, which affected EEG power density in the wake state. However, this phenomenon mainly occurred in vSUB-hM3Dq mice and was significantly reduced in vSUB^{NAc}-, vSUB^{LH}-, and vSUB^{PFC}-hM3Dq mice. Additionally, focal optogenetic activation of vSUB glutamatergic neurons in ChR2 mice also evoked epilepsy (picture not shown), but seizures occurred more easily following high- (20 Hz) versus low- (5–10 Hz) frequency stimulation. We speculate that the occurrence of epilepsy is related to the number of activated vSUB glutamatergic neurons, which is worth further study.

We used only male mice in the study, which is a limitation of the experimental design. Previous findings have shown that the high hormone phase of proestrus in female mice increases wakefulness and decreases both NREM and REM sleep compared with other estrous phases and to males [68]. Therefore, the implications of sex disparities in sleep-wake regulation of vSUB neurons deserve further study. In the current study, we used optogenetic methods to investigate the neural circuit mechanisms in sleep-wake regulation, but potential confounds of the optical stimulations should be considered. These include the antidromic effects on the axons of vSUB neurons as well as the optical stimulation of fibers that pass through the illuminated region. Thus, we combined optogenetic viral tools with retrograde-targeted chemogenetic viral tools to overcome this limitation. Besides, we used AAV under the control of the CaMKII α promoter in different experimental protocols. Pharmacological manipulation [69] and electrophysiological recordings [20, 43] suggest that laser stimulation within NAc or LH is sufficient to elicit glutamatergic, monosynaptic excitatory postsynaptic currents (EPSCs) after injection of CaMKII α -ChR2-eYFP virus into the vHPC. Moreover, recent research using the Camk2 α -Cre mouse line targets excitatory neurons in the CA1 or SUB [4]. Therefore, we believe that the CaMKII α promoter targets viral infection to glutamatergic neurons within the vSUB.

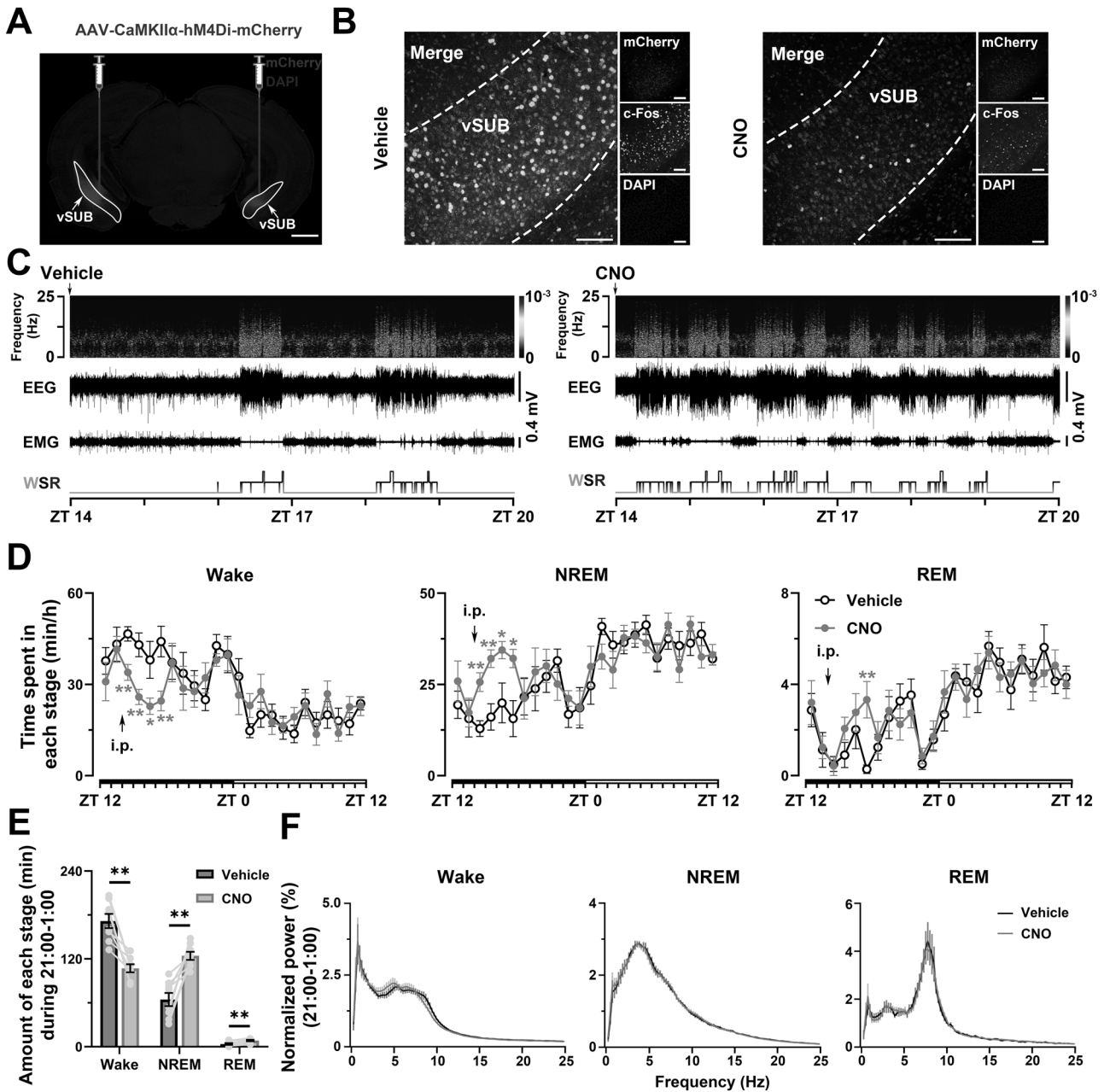


Fig. 5 Chemogenetic inhibition of vSUB glutamatergic neurons decreases wakefulness. **A** Representative image of virus injection at the vSUB. Scale bar: 1 mm. **B** Representative images of mCherry/c-Fos/DAPI immunofluorescence in vSUB after vehicle or CNO injection at ZT 14 in a hM4Di mouse. **C** Typical examples of EEG power spectrum, EEG/EMG traces, and hypnograms over 6 h after vehicle or CNO injection at ZT 14 in a hM4Di mouse. **D** Time-course changes in wakefulness, NREM sleep and REM sleep after administration of vehicle or CNO (n = 8, two-way RM ANOVA between compound injected and time; Wake: $F_{1,14} = 1.58$, $P = 0.046$; NREM: $F_{1,14} = 1.73$, $P = 0.021$; REM: $F_{1,14} = 0.88$, $P = 0.622$, followed by Sidak's post hoc tests). **E** The total time spent in each stage during 4 h after vehicle or CNO injection (n = 8, paired t test; Wake: $t_{14} = 5.20$, $P = 0.001$; NREM: $t_{14} = 5.07$, $P = 0.001$; REM: $t_{14} = 3.57$, $P = 0.009$). **F** EEG power density of wakefulness, NREM sleep, and REM sleep for 4 h after vehicle or CNO administration (n = 6, two-way ANOVA; not statistically significant). Data are represented as mean \pm SEM ($*P < 0.05$, $**P < 0.01$).

In conclusion, our results reveal a new mechanism of how vSUB regulates sleep–wake cycle and provide a new potential treatment target for sleep–wake disorders.

DATA AVAILABILITY

The raw data generated in this study have been deposited in the Figshare database under accession code: <https://doi.org/10.6084/m9.figshare.25658037>.

REFERENCES

- Mueller NK, Dolgas CM, Herman JP. Stressor-selective role of the ventral subiculum in regulation of neuroendocrine stress responses. *Endocrinology*. 2004;145:3763–68.
- Fanselow MS, Dong HW. Are the dorsal and ventral hippocampus functionally distinct structures? *Neuron*. 2010;65:7–19.
- Yan JJ, Ding XJ, He T, Chen AX, Zhang W, Yu ZX, et al. A circuit from the ventral subiculum to anterior hypothalamic nucleus GABAergic neurons essential for anxiety-like behavioral avoidance. *Nat Commun*. 2022;13:7464.

4. Sun YJ, Jin SQ, Lin XX, Chen LJ, Qiao X, Jiang L, et al. CA1-projecting subiculum neurons facilitate object–place learning. *Nat Neurosci*. 2019;22:1857–70.
5. Torromino G, Autore L, Khalil V, Mastroianni V, Griguoli M, Pignataro A, et al. Offline ventral subiculum–ventral striatum serial communication is required for spatial memory consolidation. *Nat Commun*. 2019;10:5721.
6. Grimm CM, Aksamaz S, Schulz S, Teutsch J, Sicinski P, Liss B, et al. Schizophrenia-related cognitive dysfunction in the Cyclin-D2 knockout mouse model of ventral hippocampal hyperactivity. *Transl Psychiatry*. 2018;8:212.
7. Meyer FF, Louilot A. Latent inhibition-related dopaminergic responses in the nucleus accumbens are disrupted following neonatal transient inactivation of the ventral subiculum. *Neuropsychopharmacology*. 2011;36:1421–32.
8. Sesack SR, Grace AA. Cortico-basal ganglia reward network: microcircuitry. *Neuropsychopharmacology*. 2010;35:27–47.
9. Sun WL, Rebec GV. Lidocaine inactivation of ventral subiculum attenuates cocaine-seeking behavior in rats. *J Neurosci*. 2003;23:10258–64.
10. Glangetas C, Fois GR, Jalabert M, Lecca S, Valentini K, Meye FJ, et al. Ventral subiculum stimulation promotes persistent hyperactivity of dopamine neurons and facilitates behavioral effects of cocaine. *Cell Rep*. 2015;13:2287–96.
11. Spiegelhalter K, Regen W, Nanovska S, Baglioni C, Riemann D. Comorbid sleep disorders in neuropsychiatric disorders across the life cycle. *Curr Psychiatry Rep*. 2013;15:364.
12. Richard JS, Charles LW, Anatol B, Itzhak F, Engel J, Jr. Sleep states differentiate single neuron activity recorded from human epileptic hippocampus, entorhinal cortex, and subiculum. *J Neurosci*. 2002;22:5694.
13. Hagan JJ, Verheijck EE, Spigt MH, Ruijt GSF. Behavioural and electrophysiological studies of entorhinal cortex lesions in the rat. *Physiol Behav*. 1992;51:255–66.
14. Macey PM, Prasad JP, Ogren JA, Moiyadi AS, Aysola RS, Kumar R, et al. Sex-specific hippocampus volume changes in obstructive sleep apnea. *Neuroimage Clin*. 2018;20:305–17.
15. De Looze C, Feeney JC, Scarlett S, Hirst R, Knight SP, Carey D, et al. Sleep duration, sleep problems, and perceived stress are associated with hippocampal subfield volumes in later life: findings from The Irish Longitudinal Study on Ageing. *Sleep*. 2022;45:zsab241.
16. Bienkowski MS, Bowman I, Song MY, Gou L, Ard T, Cotter K, et al. Integration of gene expression and brain-wide connectivity reveals the multiscale organization of mouse hippocampal networks. *Nat Neurosci*. 2018;21:1628–43.
17. Wee RWS, MacAskill AF. Biased connectivity of brain-wide inputs to ventral subiculum output neurons. *Cell Rep*. 2020;30:3644–54.
18. O'Mara SM, Commins S, Anderson M, Gigg J. The subiculum: a review of form, physiology and function. *Prog Neurobiol*. 2001;64:129–55.
19. Floresco SB, Todd CL, Grace AA. Glutamatergic afferents from the hippocampus to the nucleus accumbens regulate activity of ventral tegmental area dopamine neurons. *J Neurosci*. 2001;21:4915–22.
20. Britt JP, Benaliouad F, McDevitt RA, Stuber GD, Wise RA, Bonci A. Synaptic and behavioral profile of multiple glutamatergic inputs to the nucleus accumbens. *Neuron*. 2012;76:790–803.
21. Marek R, Jin J, Goode TD, Giustino TF, Wang Q, Acca GM, et al. Hippocampus-driven feed-forward inhibition of the prefrontal cortex mediates relapse of extinguished fear. *Nat Neurosci*. 2018;21:384–92.
22. Hsu TM, Hahn JD, Konanur VR, Noble EE, Suarez AN, Thai J, et al. Hippocampus ghrelin signaling mediates appetite through lateral hypothalamic orexin pathways. *eLife*. 2015;4:e11190.
23. Peleg-Raibstein D, Feldon J. Effects of dorsal and ventral hippocampal NMDA stimulation on nucleus accumbens core and shell dopamine release. *Neuropharmacology*. 2006;51:947–57.
24. Taepavaraprak P, Howland JG, Ahn S, Phillips AG. Neural circuits engaged in ventral hippocampal modulation of dopamine function in medial prefrontal cortex and ventral striatum. *Brain Struct Funct*. 2008;213:183–95.
25. Léna I, Parrot S, Deschaux O, Muffat-Joly S, Sauvinet V, Renaud B, et al. Variations in extracellular levels of dopamine, noradrenaline, glutamate, and aspartate across the sleep–wake cycle in the medial prefrontal cortex and nucleus accumbens of freely moving rats. *J Neurosci Res*. 2005;81:891–99.
26. Luo YJ, Li YD, Wang L, Yang SR, Yuan XS, Wang J, et al. Nucleus accumbens controls wakefulness by a subpopulation of neurons expressing dopamine D1 receptors. *Nat Commun*. 2018;9:1576.
27. Justinussen JL, Egebjerg C, Kornum BR. How hypocretin agonists may improve the quality of wake in narcolepsy. *Trends Mol Med*. 2023;29:61–69.
28. Yamashita T, Yamanaka A. Lateral hypothalamic circuits for sleep–wake control. *Curr Opin Neurobiol*. 2017;44:94–100.
29. Mashour GA, Pal D, Brown EN. Prefrontal cortex as a key node in arousal circuitry. *Trends Neurosci*. 2022;45:722–32.
30. Rahimi S, Joyce L, Fenzl T, Drexel M. Crosstalk between the subiculum and sleep–wake regulation: a review. *J Sleep Res*. 2024:e14134. <https://doi.org/10.1111/jsr.14134>. Online ahead of print.
31. Brown RE, Basheer R, McKenna JT, Strecker RE, McCarley RW. Control of sleep and wakefulness. *Physiol Rev*. 2012;92:1087–187.
32. Eban-Rothschild A, Appelbaum L, de Lecea L. Neuronal mechanisms for sleep/wake regulation and modulatory drive. *Neuropsychopharmacology*. 2018;43:937–52.
33. Sulaman BA, Wang S, Tyan J, Eban-Rothschild A. Neuro-orchestration of sleep and wakefulness. *Nat Neurosci*. 2023;26:196–212.
34. Rayan A, Agarwal A, Samanta A, Severijnen E, van der Meij J, Genzel L. Sleep scoring in rodents: Criteria, automatic approaches and outstanding issues. *Eur J Neurosci*. 2022;59:526–553.
35. Traut J, Mengual JP, Meijer EJ, McKillop LE, Alfonsa H, Hoerder-Suabedissen A, et al. Effects of clozapine-N-oxide and compound 21 on sleep in laboratory mice. *eLife*. 2023;12:e84740.
36. Urien L, Cohen S, Howard S, Yakimov A, Nordlicht R, Bauer EP. Aversive contexts reduce activity in the ventral subiculum–BNST pathway. *Neuroscience*. 2022;496:129–40.
37. Floresco SB. The nucleus accumbens: an interface between cognition, emotion, and action. *Annu Rev Psychol*. 2015;66:25–52.
38. Adhikari A, Topiwala MA, Gordon JA. Synchronized activity between the ventral hippocampus and the medial prefrontal cortex during anxiety. *Neuron*. 2010;65:257–69.
39. Schoenfeld TJ, Kloth AD, Hsueh B, Runkle MB, Kane GA, Wang SS-H, et al. Gap junctions in the ventral hippocampal-medial prefrontal pathway are involved in anxiety regulation. *J Neurosci*. 2014;34:15679–88.
40. Parfitt GM, Nguyen R, Bang JY, Aqrabawi AJ, Tran MM, Seo DK, et al. Bidirectional control of anxiety-related behaviors in mice: role of inputs arising from the ventral hippocampus to the lateral septum and medial prefrontal cortex. *Neuropsychopharmacology*. 2017;42:1715–28.
41. Padilla-Coreano N, Bolkan SS, Pierce GM, Blackman DR, Hardin WD, Garcia-Garcia AL, et al. Direct ventral hippocampal-prefrontal input is required for anxiety-related neural activity and behavior. *Neuron*. 2016;89:857–66.
42. Felix-Ortiz AC, Beyeler A, Seo C, Leppla CA, Wildes CP, Tye KM. BLA to vHPC inputs modulate anxiety-related behaviors. *Neuron*. 2013;79:658–64.
43. Jimenez JC, Su K, Goldberg AR, Luna VM, Biane JS, Ordek G, et al. Anxiety cells in a hippocampal-hypothalamic circuit. *Neuron*. 2018;97:670–83.
44. Adhikari A, Topiwala MA, Gordon JA. Single units in the medial prefrontal cortex with anxiety-related firing patterns are preferentially influenced by ventral hippocampal activity. *Neuron*. 2011;71:898–910.
45. Cornwall BR, Arkin N, Overstreet C, Carver FW, Grillon C. Distinct contributions of human hippocampal theta to spatial cognition and anxiety. *Hippocampus*. 2012;22:1848–59.
46. Bannerman DM, Deacon RMJ, Offen S, Friswell J, Grubb M, Rawlins JNP. Double dissociation of function within the hippocampus: Spatial memory and hyponeophagia. *Behav Neurosci*. 2002;116:884–901.
47. Arrigoni E, Chee MJS, Fuller PM. To eat or to sleep: that is a lateral hypothalamic question. *Neuropharmacology*. 2019;154:34–49.
48. Lee MG, Hassani OK, Jones BE. Discharge of identified orexin/hypocretin neurons across the sleep–waking cycle. *J Neurosci*. 2005;25:6716–20.
49. Tsunematsu T, Ueno T, Tabuchi S, Inutsuka A, Tanaka KF, Hasuwa H, et al. Optogenetic manipulation of activity and temporally controlled cell-specific ablation reveal a role for MCH neurons in sleep/wake regulation. *J Neurosci*. 2014;34:6896–909.
50. Vetrivelan R, Kong D, Ferrari LL, Arrigoni E, Madara JC, Bandaru SS, et al. Melanin-concentrating hormone neurons specifically promote rapid eye movement sleep in mice. *Neuroscience*. 2016;336:102–13.
51. Hahn JD, Swanson LW. Connections of the juxtaventromedial region of the lateral hypothalamic area in the male rat. *Front Syst Neurosci*. 2015;9:66.
52. Hahn JD, Swanson LW. Distinct patterns of neuronal inputs and outputs of the juxtaparaventricular and supraformal regions of the lateral hypothalamic area in the male rat. *Brain Res Rev*. 2010;64:14–103.
53. Folgueira C, Beiroa D, Porteiro B, Duquenne M, Puighermanal E, Fondevila MF, et al. Hypothalamic dopamine signalling regulates brown fat thermogenesis. *Nat Metab*. 2019;1:811–29.
54. Mogenson GJ, Yang CR. The contribution of basal forebrain to limbic-motor integration and the mediation of motivation to action. *Adv Exp Med Biol*. 1991;295:267–90.
55. Eban-Rothschild A, Rothschild G, Giardino WJ, Jones JR, de Lecea L. VTA dopaminergic neurons regulate ethologically relevant sleep–wake behaviors. *Nat Neurosci*. 2016;19:1356–66.
56. Baimel C, McGarry LM, Carter AG. The projection targets of medium spiny neurons govern cocaine-evoked synaptic plasticity in the nucleus accumbens. *Cell Rep*. 2019;28:2256–63.
57. Zinsmaier AK, Dong Y, Huang YH. Cocaine-induced projection-specific and cell type-specific adaptations in the nucleus accumbens. *Mol Psychiatry*. 2022;27:669–86.

58. Oishi Y, Suzuki Y, Takahashi K, Yonezawa T, Kanda T, Takata Y, et al. Activation of ventral tegmental area dopamine neurons produces wakefulness through dopamine D2-like receptors in mice. *Brain Struct Funct.* 2017;222:2907–15.
59. Briand LA, Gritton H, Howe WM, Young DA, Sarter M. Modulators in concert for cognition: modulator interactions in the prefrontal cortex. *Prog Neurobiol.* 2007;83:69–91.
60. Hoover WB, Vertes RP. Anatomical analysis of afferent projections to the medial prefrontal cortex in the rat. *Brain Struct Funct.* 2007;212:149–79.
61. Floresco SB, Grace AA. Gating of hippocampal-evoked activity in prefrontal cortical neurons by inputs from the mediodorsal thalamus and ventral tegmental area. *J Neurosci.* 2003;23:3930–43.
62. Ott T, Nieder A. Dopamine and cognitive control in prefrontal cortex. *Trends Cogn Sci.* 2019;23:213–34.
63. Li YD, Luo YJ, Xu W, Ge J, Cherasse Y, Wang YQ, et al. Ventral pallidal GABAergic neurons control wakefulness associated with motivation through the ventral tegmental pathway. *Mol Psychiatry.* 2021;26:2912–28.
64. Han Y, Shi YF, Xi W, Zhou R, Tan ZB, Wang H, et al. Selective activation of cholinergic basal forebrain neurons induces immediate sleep-wake transitions. *Curr. Biol.* 2014;24:693–98.
65. Boucetta S, Cissé Y, Mainville L, Morales M, Jones BE. Discharge profiles across the sleep–waking cycle of identified cholinergic, GABAergic, and glutamatergic neurons in the pontomesencephalic tegmentum of the rat. *J Neurosci.* 2014;34:4708.
66. Ren SC, Wang YL, Yue FG, Cheng XF, Dang RZ, Qiao QC, et al. The paraventricular thalamus is a critical thalamic area for wakefulness. *Science.* 2018;362:429–34.
67. Fei F, Wang X, Xu C, Shi J, Gong Y, Cheng H, et al. Discrete subicular circuits control generalization of hippocampal seizures. *Nat Commun.* 2022;13:5010.
68. Swift KM, Keus K, Echeverria CG, Cabrera Y, Jimenez J, Holloway J, et al. Sex differences within sleep in gonadally intact rats. *Sleep.* 2020;43:zsz289.
69. Bagot RC, Parise EM, Peña CJ, Zhang HX, Maze I, Chaudhury D, et al. Ventral hippocampal afferents to the nucleus accumbens regulate susceptibility to depression. *Nat Commun.* 2015;6:7062.

ACKNOWLEDGEMENTS

We thank the following individuals for technical assistance to this work: Xiao Tan, Yuyang Ni, Meifang Ma, Zhenzhen Tian, Caijun Dong, Shuping Fang, Wenting Yang, Hongjun Liu, Feiyang Zhang, Yun Wang, Wei Jing.

AUTHOR CONTRIBUTIONS

X-FZ, H-BX and L-LB designed the experiments. X-FZ, Y-DL, Yue Li, Ying Li and DX collected and analysed the data. X-FZ, and Y-DL discussed the results and wrote the paper.

FUNDING

This study was supported by National Natural Science Foundation of China (grants: 81771819 and 32071140), the Scientific Research Project of Hubei Provincial Health Commission (grant: WJ2019H058), the Scientific Research Project of Traditional Chinese Medicine of Hubei Province (ZY2023Q032) and Research Grant of Guangdong Province Key Laboratory of Psychiatric Disorders (N202301).

COMPETING INTERESTS

The authors declare no competing interests.

ADDITIONAL INFORMATION

Supplementary information The online version contains supplementary material available at <https://doi.org/10.1038/s41386-024-01875-6>.

Correspondence and requests for materials should be addressed to Lin-Lin Bi or Hai-Bo Xu.

Reprints and permission information is available at <http://www.nature.com/reprints>

Publisher's note Springer Nature remains neutral with regard to jurisdictional claims in published maps and institutional affiliations.

Springer Nature or its licensor (e.g. a society or other partner) holds exclusive rights to this article under a publishing agreement with the author(s) or other rightsholder(s); author self-archiving of the accepted manuscript version of this article is solely governed by the terms of such publishing agreement and applicable law.